Traction Control of Electric Vehicle: Basic Experimental Results Using the Test EV "UOT Electric March"

Yoichi Hori, *Member, IEEE*, Yasushi Toyoda, and Yoshimasa Tsuruoka

Abstract— The most distinct advantage of the electric vehicle is its quick and precise torque generation. However, most electric vehicles developed to date have not yet utilized it. In this paper, two novel traction control techniques of an electric vehicle using this advantage are proposed. One is the model-following control and the other is the optimal slip ratio control. The basic effectiveness of the proposed methods is demonstrated by real experiments using the dc-motor-driven test vehicle "UOT (University of Tokyo) Electric March."

Index Terms— Antilock braking system, electric vehicle, estimation, model following control, motion control, road condition estimation, robust control, slip ratio control, traction control.

I. Introduction

RECENTLY, many electric vehicles (EV's) have been developed [1], mainly to solve environmental and energy problems caused by the use of internal combustion engine vehicles (ICV's). Some of them already have enough performance, even in practical use. However, they have not yet utilized the most remarkable advantage of the EV. The generated torque of electric motors can be controlled much more quickly and precisely than that of internal combustion engines [13]. It is well known that the adhesion characteristics between tire and road surface are greatly affected by the control of the traction motor. This means that the vehicle stability and safety can be greatly improved by controlling the motor torque appropriately. If we can use special low-drag tires with smaller energy loss, the range of one battery charge will be greatly expanded.

In this paper, we will propose some novel traction control techniques, which can be realized only by utilizing the electric motor's quick torque response [14]. They are the model-following control (MFC) and the optimal slip ratio control. By using a newly developed dc-motor-driven test vehicle, the "UOT (University of Tokyo) Electric March," we will show some successful experimental results. In order to achieve the

Y. Hori and Y. Tsuruoka are with the Department of Electrical Engineering, University of Tokyo, Tokyo, 113-8656 Japan (e-mail: hori@hori.t.u-tokyo.ac.jp).

Y. Toyoda was with the Department of Electrical Engineering, University of Tokyo, Tokyo, 113 Japan. He is now with the Power Device Development Center, Hitachi Works, Hitachi Corporation, Hitachi, Ibaraki, 319-1221 Japan.
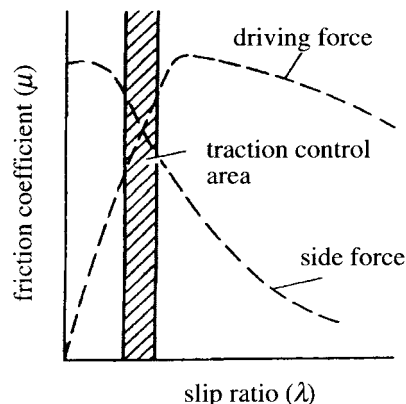
Fig. 1. Characteristics of driving and lateral forces.

best control performance, the estimation method of the road surface condition is proposed, and its basic realizability is shown by actual experiments.

II. State of the Art of Traction Control

Traction control is the control which suppresses tire slip when the vehicle is accelerating on an icy road, for example. It is realized by controlling the traction force. As a result, driving and cornering performance are improved.

We should consider two forces acting on the vehicle body. They are the driving (longitudinal) and side (lateral) forces [2]. As depicted in Fig. 1, these force characteristics strongly depend on the slip ratio λ. In acceleration, λ is defined by (1), where V_w and V are the wheel and vehicle speeds:

$$\lambda = (V_w - V)/V_w. \tag{1}$$

The side force takes its maximum value when $\lambda = 0$ and becomes quickly smaller for bigger λ. If λ increases by a sudden decrease of road friction, the side force becomes drastically smaller. This causes serious problems, including drift-out in front-wheel-driven cars, spin in rear-wheel-driven cars, and drift-out with rotation in four-wheel-driven cars. Such a loss of cornering force is extremely dangerous. The average traction force is also decreased.

We think that traction control can be classified into the following two steps.

TABLE I
COMPARISON OF TRACTION CONTROLS FOR ICV

	controllability	response	cost	operation feeling	total
engine control	good	fair	excellent	fair	good
brake control	good	excellent	excellent	poor	fair
mission control	fair	poor	excellent	fair	poor
engine + mission controls	good	fair	good	fair	fair
engine + brake controls	excellent	excellent	good	good	excellent

Fig. 2. Block diagram of MFC.

1) *Longitudinal control*—For example, this is the adhesion improvement control to prevent slip. This is achieved by controlling the traction force.
2) *Lateral control*—For example, this is the yaw control to keep the yaw motion at zero. At present, this is achieved mainly by controlling the steering angle.

For the lateral control, the steering angle of the front wheels is the dominant control input [3]–[5]. Such a technique is already well developed for the ICV. Most of these results can be applied to the EV in a much more sophisticated manner. For example, by introducing the independent control of four in-wheel motors, we can realize completely a new motion control of the EV [6] and [7]. However, in this paper, as our first attempt, we focus our discussion on *longitudinal control*. To realize the effective traction control system, we need a sophisticated mechanism to quickly reduce the excessive driving torque. In the ICV, this is realized mainly by the following three techniques.

1) *Engine Control*—Engine torque itself is suppressed. To reduce the air supply is the basic technique, but for quicker response, advanced techniques like fuel-cut and spark timing shift are used together.
2) *Brake Control*—Wheel rotation itself can be stopped by braking. This method has quicker response than the engine control. Independent control of left and right tires is effective for μ-split braking. Brake control should be used together with the engine control, because brake parts often have thermal problems.
3) *Mission Control*—Driving torque of the slipping tire is transferred to the nonslipping tire. This technique is effective for μ-split road. As the total torque cannot be reduced, this mission control should be applied together with the engine control.

Table I summarizes the advantages and disadvantages of these techniques.

III. ADVANTAGE OF EV

The electric vehicle has the following great advantages for the realization of high-performance traction control.

1) *Low Cost*—In the case of an ICV, the above-mentioned techniques need additional costly hardware, e.g., throttle and brake actuators. The EV does not need anything
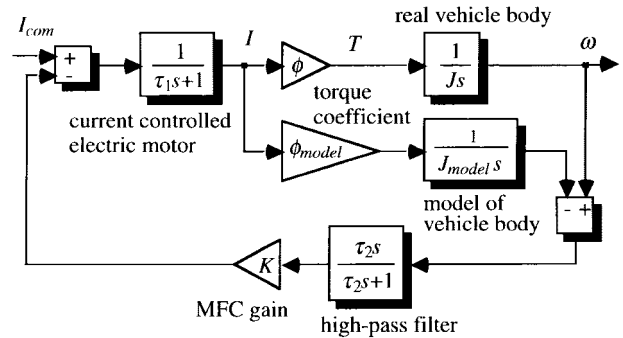
more. Traction control can be realized only by software. Even the lowest cost "basic car" can have high-performance traction control.
2) *Quick Response*—In the ICV, more than 200 ms are needed to open the throttle actuator. The actual response is much slower, because additional delay in the mechanical system must be included. In contrast, the response time of the electric motor torque is less than 10 ms.
3) *Easy Controller Design*—In the ICV, unknown strong nonlinearity lies in the transfer characteristics from the control input (for example, air valve angle to engine, oil pressure of brake system, etc.) to the generated torque. This makes it difficult to construct a mathematical model for controller design. In the EV, by applying simple current control, the generated torque is exactly proportional to the torque command.

IV. MFC

In this paper, we propose two control strategies: "*MFC*" and "*optimal slip ratio control*." MFC is the starting point of our research project of "the control of an EV," and its basic feasibility is demonstrated here by actual experiment.

A. Principle of MFC

Fig. 2 shows the block diagram of MFC. I_{com} is the current command proportional to the acceleration pedal angle. ω is the rotational speed of the driving shaft. ω increases drastically when the tire slips. Although the vehicle dynamics, including tire characteristics and road surface friction, are very complicated, if we introduce the slip ratio λ, the vehicle body can be seen as one inertia system having the equivalent inertia moment of

$$J = J_w + Mr^2(1 - \lambda). \qquad (2)$$

Here, J_w, M, and r are the shaft inertia moment, vehicle weight, and tire radius, respectively. Equation (2) means that, when slip occurs, the vehicle seems lighter. Therefore, we use the following inertia moment with $\lambda = 0$ in the reference model:

$$J_{\text{model}} = J_w + Mr^2. \qquad (3)$$

When there is no slip, actual J is almost equal to J_{model}. A signal is not generated from the MFC controller. If the tire
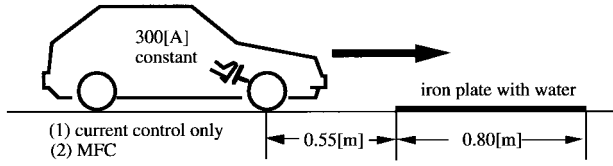
Fig. 3. Slip experiment.

slips, the actual wheel speed ω increases immediately. The model wheel speed does not increase. By feeding the speed difference back to the motor current command, the actual motor torque is reduced quickly, and it induces readhesion.

As this control function is needed only in a relatively higher frequency region, we used a high-pass filter on the feedback pass. In actual implementation, in order to avoid the offset problem of an integrator, two high-pass filters are inserted before taking the difference between the actual and the model speeds. When the feedback torque from the MFC blocks is positive, it is forced to be zero.

B. Experimental Result of the MFC

Fig. 3 shows the slip experiment using the UOT Electric March. We used iron plates as a slippery road surface. Water is scattered to reduce the friction coefficient. The vehicle is accelerated by the constant current command of 300 A. The feedback gain K in Fig. 2 is 30. The front wheels are on the slippery area between $t = 1.25$ and 1.7 s.

Experimental results are given in Fig. 4. We can see that the MFC can reduce the motor current effectively when the vehicle goes onto the slippery area, and then the slip ratio is kept much lower compared to the case of current control only. Some vibration observed in the current waveform in Fig. 4(a) can be suppressed in the future.

V. OPTIMAL SLIP RATIO CONTROL

The MFC is a very rough approach, although it has been shown that the motor control is really effective for adhesion improvement. If we want more exactly to regulate the slip ratio within the desired range, a more precise approach is needed. Fig. 5 shows the idea of the optimal slip ratio control developed from this viewpoint. When the optimal slip ratio is decided by the road condition estimator, the slip ratio controller receives the command and tries to realize it.

A. Vehicle Model

We assume that the two motor torques and friction forces are the same in left and right tires and that the rolling and air frictions are small enough. In Fig. 6, the kinematic equations of the wheel and vehicle take the forms

$$(F_m - F_d)\frac{1}{M_w s} = V_w \quad (4)$$

and

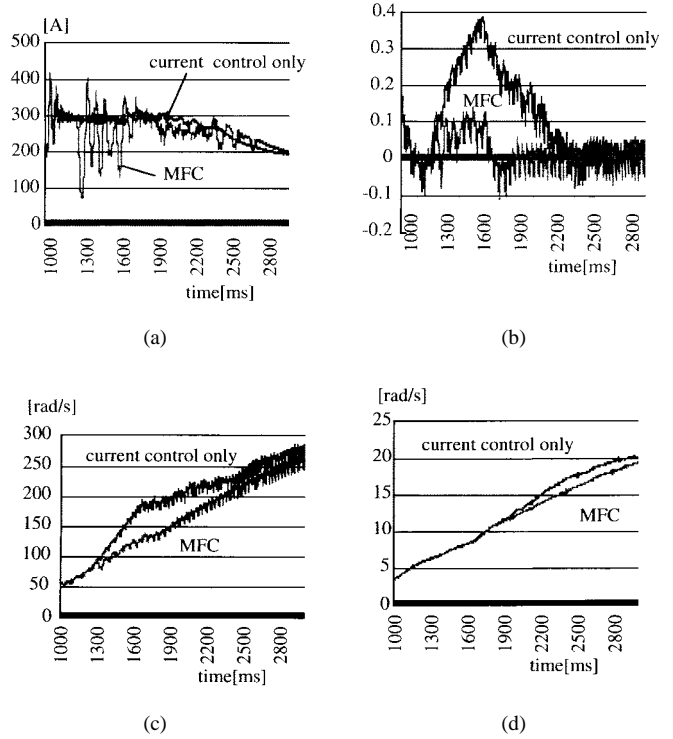$$F_d \frac{1}{Ms} = V \quad (5)$$

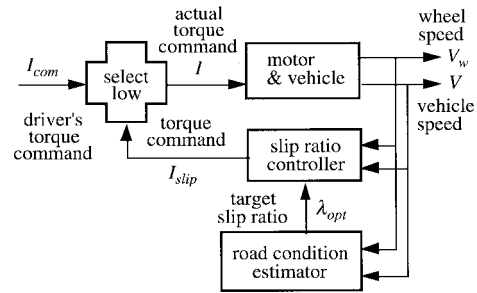Fig. 4. Experimental results of MFC. (a) Motor current. (b) Slip ratio. (c) Wheel speed. (d) Vehicle speed.

Fig. 5. Block diagram of the optimal slip ratio controller.

where

F_m motor torque (force equivalent);
F_d friction force;
M_w wheel inertia (mass equivalent);
M vehicle weight.

The friction force between the road and wheel is given by

$$F_d = N\mu(\lambda) \quad (6)$$

where N is the vertical force given by $N = Mg$.

From (1), the following perturbation system is derived:

$$\Delta\lambda = \frac{\partial\lambda}{\partial V}\Delta V + \frac{\partial\lambda}{\partial V_w}\Delta V_w = -\frac{1}{V_{w0}}\Delta V + \frac{V_0}{V_{w0}^2}\Delta V_w \quad (7)$$

where V_{w0} and V_0 are the wheel and vehicle speeds at the operational point. The friction force is represented using a,
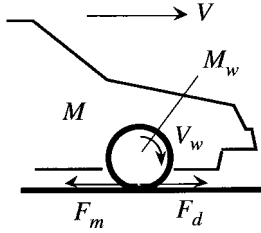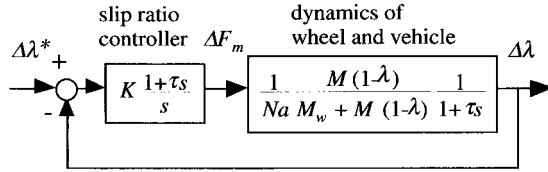
Fig. 6.   Vehicle model.

Fig. 7.   Slip ratio controller.

Fig. 8.   Nominal slip ratio is given by $a = 1$.

the gradient of $\mu - \lambda$ curve, as

$$\Delta\mu = a\Delta\lambda. \tag{8}$$

By combining (7) and (8) with the perturbation forms of (4) and (5), the transfer function from the motor torque to the slip ratio is finally given by

$$\frac{\Delta\lambda}{\Delta F_m} = \frac{1}{Na}\frac{M(1-\lambda)}{M_w + M(1-\lambda)}\frac{1}{1+\tau s} \tag{9}$$

where the time constant τ is given by (10), which is proportional to the wheel speed V_{w0}:

$$\tau = \frac{1}{Na}\frac{MM_wV_{w0}}{M_w + M(1-\lambda)}. \tag{10}$$

The typical value of τ in our experimental vehicle is 150–200 ms when $a = 1$ and the vehicle speed is around 10 km/h. Note that a can be negative in the right-hand side of the peak point of the $\mu - \lambda$ curve.

B. Design of Slip Ratio Controller

We used a simple proportional integral (PI) controller with a variable gain as the slip ratio controller given by (11), as depicted in Fig. 7. Its nominator compensates for the pole of (9). The integral gain is constant and the proportional gain is proportional to the vehicle speed:

$$K\frac{1+\tau s}{s}. \tag{11}$$

Finally, the transfer function from the slip ratio command to the actual slip ratio becomes

$$\frac{\Delta\lambda}{\Delta\lambda^*} = \frac{1}{1 + Na\dfrac{M_w + M(1-\lambda)}{M(1-\lambda)}\dfrac{1}{K}s}. \tag{12}$$

If $\lambda \ll 1$, this is a simple first-order delay characteristic with a time constant which can be adjusted by K. Here, we put this response time from 50–100 ms.
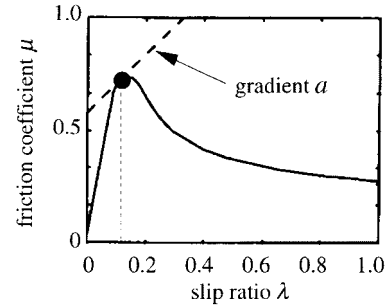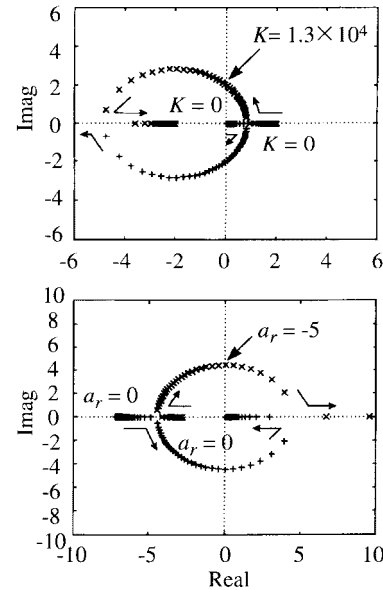

Fig. 9.   Root locus against parameter variation.

Fig. 8 shows the nominal slip ratio used in the slip ratio controller. We defined it by $a = 1$. The point of $a = 1$ is located just in the left side of the peak and is stable. Both of the longitudinal and lateral forces are kept still high.

C. Robustness to Parameter Variation

Because the actual system parameters change widely, we should investigate the robustness of the slip ratio controller. Fig. 9 draws the root locus to continuous change of K and a_r (actual a). From the figures, we can see that the roots move to the left-half plane when the controller gain K increases. It is interesting that this controller stabilizes the system, even when actual a is negative, although the roots move toward the unstable region.

D. Simulation of Slip Ratio Control

Fig. 10 shows the vehicle model we used in the simulation. T represents the motor torque and r the total gear ratio of the drive train. F_d represents the summation of traction force transferred to the contact point of tire and road surface. It is the product of the traction coefficient μ and $N = Mg$, the
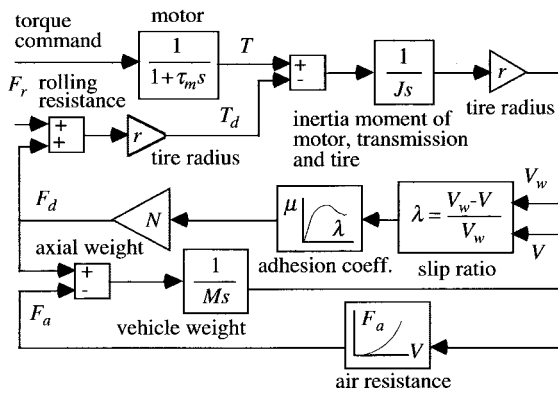
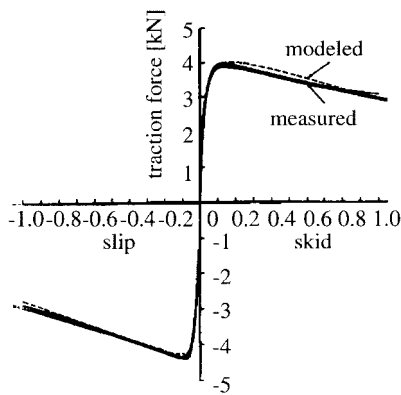Fig. 10.   Vehicle model used in the simulation.

Fig. 11. μ–λ characteristics used in the simulation.

Fig. 12.   Simulation of the slip ratio control.

vertical load on the contact point. μ is defined as the function of λ, which is given by the measured curve shown in Fig. 11.

Fig. 12 is the simulation result. The response time of the slip ratio controller is set to be 100 ms. We can see good response characteristics.

E. Experimental Results of Slip Ratio Control

Fig. 13 shows the experimental results of the slip ratio control using the laboratory-made experimental EV "UOT Electric March." Here, the response time is 50 ms and the target slip ratio is 0.1 in Fig. 13(a) and is changed stepwise from 0.3 to 0.1 in Fig. 13(b).

Basically, we can see fairly good performance, but there are some problems. First, the actual value of a was much smaller than the nominal value 1. This made the response time longer than the designed value. Next, in Fig. 13(b), we see an undershoot to the slip ratio command of 0.1. This is because the motor controller we used is only a 1-quadrant chopper, which cannot absorb the motor current.

VI. ESTIMATION OF ROAD CONDITION

In the previous section, we showed the effective slip ratio control. The next problem is how to give the optimal slip ratio to the slip ratio controller.
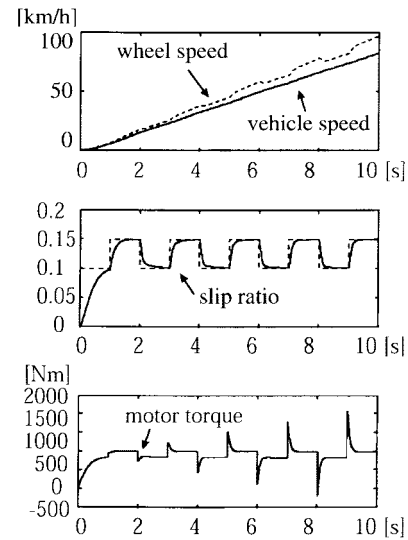
We showed the relation between the slip ratio λ and the friction coefficient μ in Figs. 1 and 11, but it varies very widely according to road surface condition, as shown in Fig. 14. It is clear that the slip ratio where the friction force takes its maximum value varies according to road condition. This means that the road condition should be estimated relatively quickly for giving the optimal slip ratio to the slip ratio control.

To know the road surface condition, we should estimate the friction coefficient [10]–[12]. If we can measure the vehicle speed directly by using the nondriven wheel, the friction coefficient μ can be obtained by (13) based on (3) and (4):

$$\mu = \frac{M}{N}\frac{dV}{dt}. \tag{13}$$

When the vehicle speed cannot be measured directly, we can estimate μ based on

$$\mu = \frac{1}{N}\left(F_m - M_w\frac{dV_w}{dt}\right). \tag{14}$$

In our case, we can use both of these methods. Fig. 15 shows the estimation result of the $\mu - \lambda$ curve of a dry asphalt road when no slip control is active. At the point around $\lambda = 0.08$, the gradient a of the μ–λ curve is about 1.

Fig. 16 shows the estimation results on a wet iron surface under the slip ratio control proposed in the previous section. Here, the optimal slip ratio is smaller than 0.05. It is also noticed that, in our experiment shown in Fig. 13(a), the actual gradient of the $\mu - \lambda$ curve at $\lambda = 0.1$ was almost -1. We can see that the slip ratio controller still works effectively, even when the operation point is unstable, but, in this case, we should have commanded a lower slip ratio.

For effective traction control, it is enough to know the gradient of the $\mu - \lambda$ curve. We are going to introduce an adaptive identification method for realization of "the optimal slip ratio control based on the estimation of the road surface condition," which is our next target.
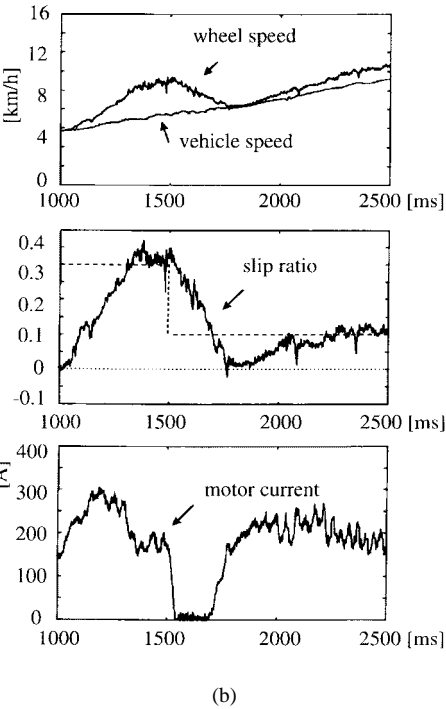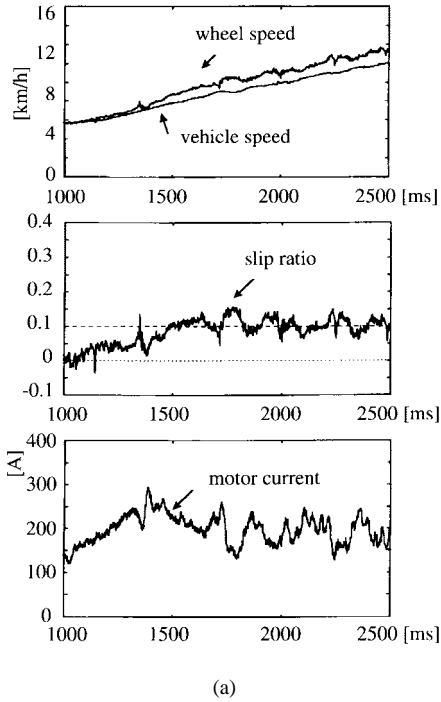
(a)

(b)

Fig. 13. Experimental results of the slip ratio control.

Fig. 14. Various road conditions.

Fig. 15. Estimation result of μ–λ curve of dry asphalt road.
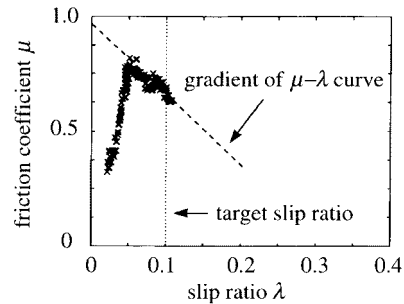
Fig. 16. Estimation result of μ–λ curve of wet iron plate under the slip ratio control.

VII. CONCLUSION

We have proposed a new field of "motion control of an EV." The EV is a very interesting object, combining the electrical and mechanical engineering fields from the viewpoint of motion control. As an example, we proposed advanced adhesion control utilizing the quick and precise torque response of the electric motor.

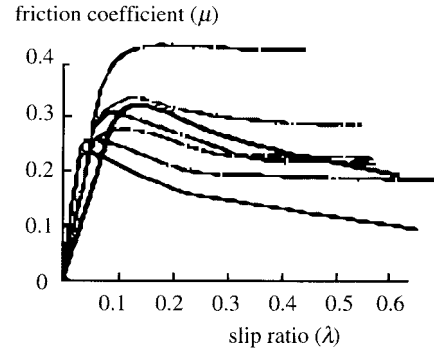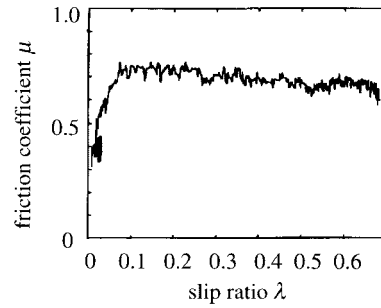We proposed the MFC and the optimal slip ratio control. We confirmed that the MFC can reduce its torque quickly when the motor speed is suddenly increased by tire slip. Next, we showed that the optimal slip ratio control has more advanced performance. Such kinds of quick control are first realized only in EV's. It is clearly shown that relatively sophisticated control theory can work well in actual experiments.

Advanced adhesion control is helpful for lateral control, like yaw disturbance attenuation [6]–[9]. This is because the proposed optimal slip ratio control keeps the tire slip within the small region. where both of the longitudinal and lateral adhesion coefficients are still high enough.

APPENDIX

Configuration of UOT Electric March: We developed a real test EV, the "UOT Electric March," as shown in Fig.
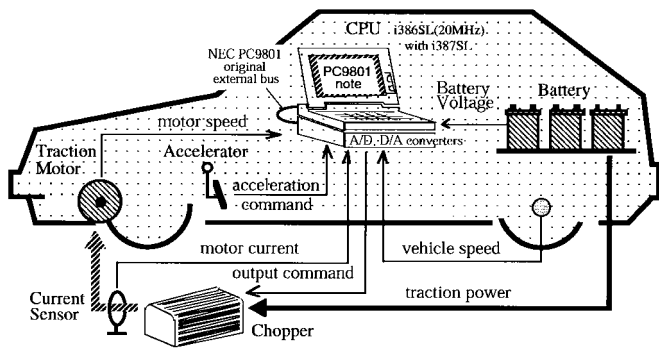
Fig. 17.   UOT Electric March.

Fig. 18.   Configuration of UOT Electric March.

TABLE II
SPECIFICATION OF UOT ELECTRIC MARCH

Conversion Base	Nissan March (Micra)
size	3785×1560×1395[mm]
weight	900[kg](batteries included)
Motor	Advanced D.C. Motors, Inc.
type	DC series wound
rated power (@120V)	19[kW](1hr.), 32[kW](5min.)
size/weight	ϕ232, length 397[mm], 65[kg]
Controller	Curtis Instruments, Inc.
type	MOSFET PWM Chopper
operating frequency	15[kHz]
rated voltage/current	120[V]/400[A]
Battery	Japan Storage Battery Co.,Ltd. GTX-130E41L
type	lead acid
voltage/capacity	72[V]/92[Ah](5hr)
weight	27.5[kg]×6
CPU	PC9801NS/T (386SL, 20MHz)
weight	3.2[kg]
A/D and D/A converters	12bit, 8ch / 12bit, 2ch
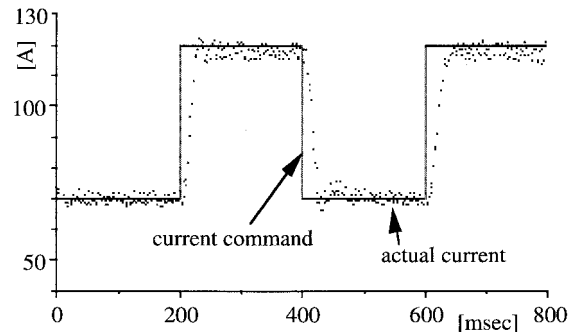
Fig. 19.   Basic experiment on the current response.

17. It is a converted car, the IC engine of which has been replaced by an electric motor.

The front two wheels are driven by a 19-kW series-wound dc motor through a 5-speed manual transmission and a differential gear. The 1-quadrant dc chopper supplies power to the motor. Its current limit is 400 A and it can produce maximum torque over 100 N·m, which is enough to perform the slip experiment. Current and speed sensors are also implemented. To detect the vehicle speed, a speed sensor is implemented in the rear wheel.

The aim of our research is not in motor control itself, but in motion control of an EV, where the type of motor is not a problem. What is required is for the traction motor to generate torque quickly enough. Our development is based on this quick and relatively precise torque generation. From this point of view, the dc motor is the easiest device to confirm our idea, in particular, for a basic experiment at a university.

Fig. 18 shows the control system of the vehicle, and Table II gives its specification. We used a note-type personal computer to realize all control algorithms. It not only executes the control algorithm and puts out the voltage command to the chopper, but also reads and records the sensor data. As the control algorithms are written by software (C-language), we can easily investigate various control strategies.

Fig. 19 shows the basic experimental results of the current controller.

REFERENCES

[1] K. Rajashekara, "History of electric vehicles in general motors," *IEEE Trans. Ind. Applicat.,* vol. 30, pp. 897–904, July/Aug. 1994.
[2] H. Sakai, *Tire Engineering.*   Tokyo, Japan: Grand-Prix, 1987.
[3] M. Ito and K. Isoda, "The present and future trends of traction control system," *Jidosha-Gijutsu, Soc. Automotive Engineers Japan,* vol. 46, no. 2, pp. 32–37, 1992.
[4] K. Ise *et al.,* "The 'Lexus' traction control (TRAC) system," Society of Automotive Engineers of Japan, Tokyo, Japan, Tech. Paper 900212, 1990.
[5] S. Yamazaki, T. Fujikawa, and I. Yamaguchi, "A study on braking and driving properties of automotive tires," *Trans. Soc. Automotive Engineers Japan,* vol. 23, no. 2, pp. 97–102, 1992.
[6] J. Ackermann, "Yaw disturbance attenuation by robust decoupling of car steering," in *Proc. 13th IFAC World Congr.,* 1996, 1996, pp. 1–6.
[7] Y. Wang and M. Nagai, "Integrated control of four-wheel-steer and yaw moment to improve dynamic stability margin," in *Proc. 35th IEEE-CDC,* 1996, pp. 1783–1784.
[8] N. Iwama *et al.,* "Active control of an automobile—Independent rear wheel torque control," *Trans. SICE,* vol. 28, no. 27, pp. 844–853, 1992.

[9] S. K. Sul and S. J. Lee, "An integral battery charger for four-wheel drive electric vehicle," *IEEE Trans. Ind. Applicat.,* vol. 31, pp. 1096–1099, Sept./Oct. 1995.

[10] C. Liu and H. Peng, "Road friction coefficient estimation for vehicle path prediction," *Vehicle System Dynamics Supplement,* vol. 25. Amsterdam, The Netherlands: Swets & Zeitlinger, 1996, pp. 413–425.

[11] A. Daiss and U. Kiencke, "Estimation of tire slip during combined cornering and braking observer supported fuzzy estimation," in *Proc. 13th IFAC World Congr.,* 1996, pp. 41–46.

[12] L. R. Ray, "Nonlinear tire force estimation and road friction identification: Simulation and experiments," *Automatica,* vol. 33, no. 10, pp. 1819–1833, 1997.

[13] T. Furnya, Y. Toyoda, and Y. Hori, "Implementation of advanced adhesion control for electric vehicle," in *Proc. IEEE Workshop Advanced Motion Control,* 1996, vol. 2, pp. 430–435.

[14] Y. Hori, Y. Toyoda, and Y. Tsuruoka, "Traction control of electric vehicle based on the estimation of road surface condition—Basic experimental results using the test EV UOT Electric Mar.," in *Proc. IEEJ-IEEE Power Conversion Conf.,* 1997, vol. 1, pp. 1–8.

Yasushi Toyoda received the B.S. and M.S. degrees in electrical engineering from the University of Tokyo, Tokyo, Japan, in 1995 and 1997, respectively.

He joined Hitachi, Ltd. in 1997 and is currently with the Power Device Development Center, Hitachi Works, Hitachi Corporation, Hitachi, Japan.

Yoshimasa Tsuruoka received the B.S. degree in 1997 in electrical engineering from the University of Tokyo, Tokyo, Japan. He is currently working as a postgraduate student in information and communication engineering.

His current research interest is natural language processing.

Yoichi Hori (S'81–M'83) received the B.S., M.S., and Ph.D. degrees in electrical engineering from the University of Tokyo, Tokyo, Japan, in 1978, 1980, and 1983, respectively.

He joined the Department of Electrical Engineering, University of Tokyo, in 1983 as a Research Associate. Since 1988, he has been an Associate Professor. During 1991–1992, he was a Visiting Researcher at the University of California, Berkeley. His research fields are control theory and its industrial applications, in particular, to motion control, mechatronics, power electronics, power systems, electric vehicles, etc.

Prof. Hori is a member of the Institute of Electrical Engineers of Japan, Japan Society of Mechanical Engineers, Society of Instrument and Control Engineers, Institute of Systems, Control and Information Engineers, Robotic Society of Japan, Japan Society of Simulation Technology, Japan Society of Mechanical Engineers, Society of Electric Vehicle Engineers, and Society of Automotive Engineers of Japan. He received the Best Transactions Paper Award for the IEEE TRANSACTIONS ON INDUSTRIAL ELECTRONICS in 1993.